crystals

MDPI

Review

Studies of Dislocations in Type Ib, Type IIa HPHT and CVD Single Crystal Diamonds

Devi Shanker Misra

Tukang Innovation Drive, IIA Technologies Pvt Ltd., Singapore 618300, Singapore; drk1955@gmail.com

Abstract: In this review, the X-ray topography results of various types of single crystal diamonds (SCDs) are reported. Dislocations and dislocation bundles are present in all types of SCDs, the only exception being type IIa high-pressure, high-temperature (HPHT) SCDs. The technology of growing HPHT type IIa SCDs has advanced to a level where the samples show almost no dislocations or dislocation bundles. However, very few groups appear to have perfected the process of HPHT growth of type IIa SCDs. There appears to be a characteristic difference in the dislocations present in type Ib HPHT and chemical vapor deposited (CVD) SCDs. The dislocations in CVD SCDs are mostly in aggregate form, while in HPHT type Ib diamonds there are line dislocations which propagate in <111> or <112> directions. The CVD SCDs growth appears to be in the early stage in terms of the control of dislocations and dislocation bundles, compared to other semiconductor wafers. The dislocations and dislocation bundles and aggregates in SCDs limit their applications in electronic and optical devices. For instance, high-power laser windows must have low dislocations and dislocation bundles. For electronic devices such as high-power diodes, dislocations reduce the breakdown voltage of SCDs, limiting their applications. The knowledge of dislocations, their identification and their origin are, therefore, of utmost importance for the applications of SCDs, be they HPHT or CVD grown.

Keywords: CVD diamonds; HPHT diamonds; Dislocations; Dislocation bundles; X-ray topography

check for updates

Citation: Misra, D.S. Studies of Dislocations in Type Ib, Type IIa HPHT and CVD Single Crystal Diamonds. *Crystals* **2023**, *13*, 657. https://doi.org/10.3390/cryst13040657

Academic Editors: Christian Giese, Peter Knittel and Xavier Vidal

Received: 13 March 2023
Revised: 3 April 2023
Accepted: 6 April 2023
Published: 11 April 2023

Copyright: © 2023 by the author. Licensee MDPI, Basel, Switzerland. This article is an open access article distributed under the terms and conditions of the Creative Commons Attribution (CC BY) license (https://creativecommons.org/licenses/by/4.0/).

1. Introduction

At present, microwave plasma chemical vapor deposition (MPCVD) is a commercially viable technique to manufacture single crystal diamonds (SCDs) for gemstones and various other technological applications [1–9]. In addition, many new applications based on nanocrystalline diamonds have emerged and are very attractive [10,11]. Methane (CH_4) and hydrogen (H_2) gases are used for CVD SCD growth. These gases employed for growth are of greater than 6N purity because advanced optical, thermal, radiation and electronic applications require SCDs with the least lattice defects such as inhomogeneities, stacking faults, dislocations, dislocation bundles, inclusions, impurities, precipitates and growth striations [2,5]. Impurities and structural defects such as dislocations lead to the deterioration of the characteristics of SCDs. For instance, nitrogen impurities reduce the mobilities of the charge carriers in SCDs drastically, while dislocation and dislocation bundles reduce SCDs' strength and optical properties, respectively [2–5]. To fabricate charge particle detectors based on SCDs, one must reduce the concentration of nitrogen impurities in SCDs to <1 ppb. Similarly, for the fabrication of high-power laser windows, the birefringence of the SCDs must be less than 10^{-4}. It is therefore critical to not only control these defects at their minimum, but also understand their origin in SCDs. Naturally occurring CH_4 contains about 1% ^{13}C isotopes of carbon, which implies that CVD SCDs contain about 10^{21}–10^{22} atoms of ^{13}C naturally in their lattices. It is natural to assume that ^{13}C atoms, being heavier, in the structure will give rise to strain in the lattice.

The interest in studying the impact of ^{13}C content on the properties of diamond was initiated by the initial work of Chrenko [12], and Banholzer and Anthony [13]. It was shown by Balholzer and Anthony [13] that more than a 50–100% increase in thermal conductivity

(K) of the SCDs occurs when the ^{13}C content of a single crystal diamond is reduced. The reduction in ^{13}C content of SCDs was brought about by a very novel method, as described in their paper [13]. Recently, the interest in the interaction between ^{13}C spin and the unpaired electron of a negatively charged $(N\text{-}V)^-$ centre has attracted widespread attention due to the interest in quantum system processing [14–16]. The shift in first-order Raman line position in an isotopically pure single crystal diamond as a function of pressure has been used to calibrate the pressure measurement in ultra-high pressure diamond anvil cells [17]. Novikov et al. [18] analysed the thermal conductivity (K) variation of CVD diamond single crystals and polycrystalline films as a function of ^{13}C content in the framework of a Debye model in the temperature range 10 K–1000 K. A detailed investigation of ^{13}C doping in large CVD SCDs had been previously reported [19].

Synchrotron X-ray rocking curve mapping measures the crystalline perfection within the volume of the single crystals. All types of SCDs—grown by the high-pressure, high-temperature (HPHT) technique, CVD and natural diamonds—have been studied using X-ray topography [1,2,19–45]. A series of rocking curve images across the volume of SCDs reveals the accumulation of dislocations, dislocation bundles and stacking faults [33]. An increase in full width at half maxima (FWHM) of the rocking curve directly correlates with the increase in the concentration of dislocations and stacking faults [19–45]. In addition to the above, X-ray topography imaging is also a popular technique to scan a sample and acquire a visualization of the above defects. Both rocking curve mapping and X-ray topography imaging are used to obtain complimentary information about the defects in different crystallographic planes of the SCDs or other single crystals [35]. The advantage of rocking curve mapping is that it can provide maps for all (111), (220) and (400) crystal planes, while XRT photographs may be clearly able to image the defects only for certain planes such as (404) [42].

X-ray topography (XRT) was introduced by A.R. Lang in 1964 to image a dislocation in diamond [22,23]. The XRT became a common experimental method to study the dislocations and stacking faults in SCDs in the 1990s as the intensity of X-ray sources increased [24,25]. Several studies were conducted on N doped high-pressure, high-temperature (HPHT) grown diamond crystals (type Ib), and various growth sectors, crystal planes, dislocations and stacking faults were imaged by changing the X-ray incidence angle in the transmission mode [25]. The XRT data of the SCDs were compared with optical birefringence [24,26]. Very high-quality type IIa SCDs synthesized by Sumiya et al. [26–28], using the HPHT method, showed very few dislocations in XRT. Sumiya et al. used defect-free diamond crystals as seeds in HPHT growth of type IIa SCDs. Several types of dislocations in type Ib HPHT diamond were studied by Moore et al. [30].

The first XRT study [31] on single crystal diamond grown by microwave plasma chemical vapor deposition (CVD) was carried out in 2008. The XRT study shows that the extended defect content of CVD layers depends on the growth sector of the HPHT seed crystal; (111) sectors contain the highest concentration of both stacking faults and dislocations but (004) sectors are relatively free of both [32]. The finding that the dislocations originate at the substrate/film interface and grow into the CVD diamond over-layers was confirmed by XRT studies by various authors [32,37,42,45].

2. Materials and Methods

A typical synchrotron X-ray topography setup for mapping rocking curves is shown in Figure 1. This diagram is used with the courtesy of Cornell High Energy Synchrotron Source (CHESS), USA, in beamline C1 [33]. The system is set up with a beam-expanding monochromator, a six-circle diffractometer (a rotatable sample stage) and a CMOS camera with real-time sample alignment facility. The system can provide angular resolution as small as 2 micro-radians, spatial resolution of 3 microns and field of view up to 7 mm. The C1 system is suitable to produce a series of 2D rocking curve images of the (111), (220) and (400) crystallographic planes of single crystals of diamond scanned around the Bragg angle with a scanning step of 0.0002° over a range of 0.025° for the entire crystal of the sample

plate. To further augment the facility, an additional rocking curve image is produced by rotating the sample by 90°. A mirror reflection image obtained by rotating the sample by 90° produces an image across (−220) crystallographic planes of the diamond crystals. Each pixel from the rocking curve image series can be extracted and tabulated to plot against the relative scan theta (θ) for the symmetric transmission geometry rocking curves for (111), (220) and (400) planes of single crystal diamond.

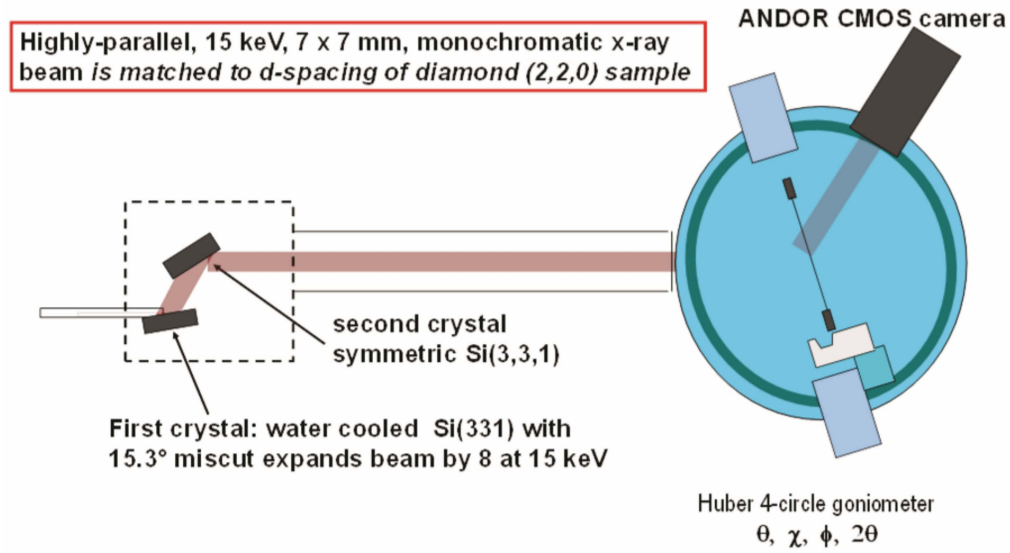


Figure 1. C1 beam line setup at Cornell High Energy Synchrotron Source (CHESS), Ithaca, NY, USA. The sample is held at room temperature. The figure is taken from ref. [33], which is published on the website of CHESS Cornell, USA, ref. [33]: Finkelstein, K.; Jones, R.; Pauling, A.; Brown, Z.; Tarun, A.; Jupitz, S.; Sagan, D.; Misra, D.S.; **2016**. http://news.chess.cornell.edu/articles/2015/Finkelstein151123.html (accessed on 7 April 2023).

The above setup can also be used to capture an XRT image of the samples. The advantage of XRT imaging is that the dislocations, dislocation bundles and stacking faults can be directly photographed. In addition, white-beam X-ray imaging can also be used to capture the XRT image. Table 1 shows a summary of the three techniques. A perfect single crystal diamond would show a homogeneous grey colour in an XRT photograph (image) with no features. Under the conditions of the full penetration of the X-rays, the dislocations would appear as a black contrast line or double lines, and, thus, the dislocations can easily be identified from an XRT photographic image. Stacking faults would appear as a dark band. A dark black aggregate would mean an intense inclusion or a twin defect where the density of defects and dislocations is very high [42].

In this report, the results of rocking curve maps, X-ray topography (XRT) images and white-beam XRT images are compiled and reported in SCDs of various types published by different authors. The dislocations, dislocation bundles and dislocation aggregates are identified in the rocking curve maps and XRT images. The results are focused mainly on HPHT and CVD grown SCDs reported in the last 25 years. The purpose of this report is to understand the occurrence of dislocations, dislocation bundles and aggregates in SCDs. The attempt is made to present the dislocation information as photographed by different techniques.

Table 1. The summary of the three XRT techniques used for dislocation mapping.

Rocking curve mapping	Rocking curve is measured for each detector pixel at a Bragg angle corresponding to a crystal plane. For each detector pixel, the FWHM is calculated from the rocking curve, and an FWHM map is created. The higher the value of FWHM, the higher the concentration of dislocations at the location. The entire crystal is illuminated with an X-ray monochromatic beam.
XRT image at a crystal plane	The sample XRT image is taken at a particular Bragg angle corresponding to a crystal plane. The image contains the dislocations, dislocation bundles and stacking faults evident with different contrast on a grey background. The entire crystal is illuminated with an X-ray monochromatic beam.
White-beam XRT imaging	The sample is illuminated perpendicular to the direction of incidence of a continuous X-ray beam. The XRT image is generated on a detector and contains the dislocations, dislocation bundles and stacking faults evident with different contrast on a grey background.

3. Results

3.1. HPHT SCDs (Type Ib)

There are two types of HPHT grown diamond crystals: (a) type Ib crystals of yellow-brown colour, and (b) white colour type IIa crystals. In type Ib yellow-brown colour crystals, the nitrogen impurities are in the range of tens of parts per million (ppm) to hundreds of ppm. The nitrogen impurities are in single substitutional form (P1 centre) [46]. The yellow-brown diamond plates are commercially available and are used often as substrates for the chemical vapor deposition (CVD) of diamond. The nitrogen uptake in yellow-brown diamond is normally from the atmosphere and the catalyst material, a carbon-dissolving metal such as iron, nickel, or cobalt, which is used for the growth of the diamond. The nitrogen uptake helps in growing clear diamonds which are inclusion-free. The image of a yellow-brown diamond crystal [47] is shown in Figure 2.

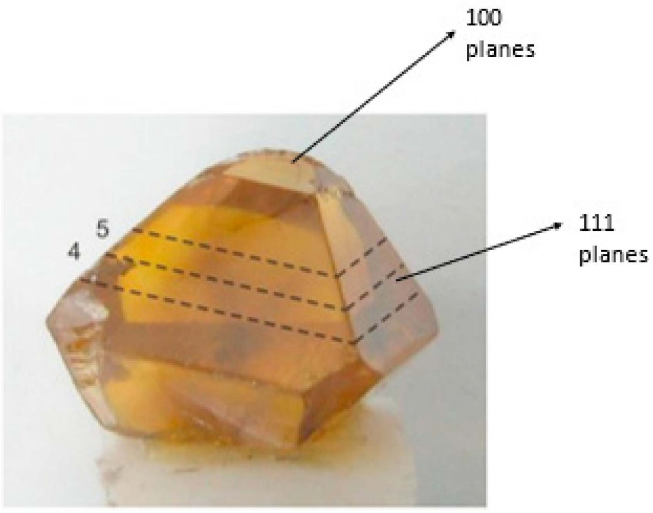


Figure 2. A yellow-brown diamond single crystal. The (100) and (111) crystallographic planes are shown. If plates are cut along dotted lines and polished, we obtain the (100) oriented plates which can be used as a substrate for CVD diamond growth. Further, the (110) crystallographic planes lie at 45 and 90°, respectively, to the (100) planes. The size of the crystal is about 4 mm × 4 mm. This image is taken from ref. [47]: Kazuchits, V.N.; Kazuchits, N.M.; Rusetskiy, M.S.; Korolik, O.V.; Konovalova, A.V.; Ignatenko, O.V. Rapid HPHT annealing of Synthetic Ib-type Diamond. *Carbon* **2021**, *174*, 180. Printed with permission from the publisher.

The sample preparation of the plates for X-ray topography is very critical for obtaining good images of the dislocations and their direction of flow. The direction of flow of a dislocation is represented by a Burgers vector [42]. If there are scratches present on the surface of the sample due to polishing or other issues, the dislocations are difficult to image, and one must infer indirectly by the rocking curve maps. Tran Thi et al. [1] took white-beam XRT images of two type Ib HPHT diamond plates of the dimensions 3 mm × 3 mm. The results showed dislocations and dislocation bundles emanating from the centre (Figure 3a). The dislocations are clearly visible in Figure 3a as thick contrast dark lines. Dislocation bundles can also be seen in the centre of the plate as well as on the edges. Figure 3b, however, shows the defects on the surface of the sample which were attributed to the mechanical origin due to the laser cutting and polishing of the samples. It is noteworthy that in the white-beam XRT measurements shown in Figure 3a, the images are captured in the (400) plane, and the dislocations are difficult to capture because of the low absorption of X-ray in diamond. A minor drawback of white-beam X-ray imaging is that images of the dislocations are not very clear and resolutions are poor. Due to this, deductions of the images of the dislocations can sometimes be subjective in white-beam XRT.

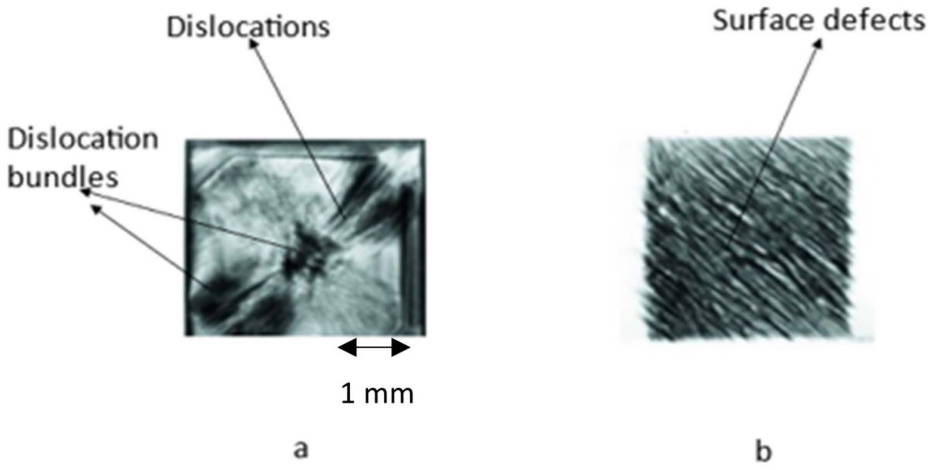


Figure 3. The XRT images of two plates of type Ib HPHT diamond of the size 3 mm × 3 mm. The dark and grey colour contrast lines in (**a**) represent dislocation lines emanating from the centre[1].The sample in (**b**) is full of surface defects perhaps of mechanical origin (please see the text). The diffraction vector (220) points along the diagonal of the figure. The image is taken from ref. [1]: Tran Thi, T.N.; Morse, J.; Caliste, D.; Fernandez, B.; Eon, D.; Härtwig, J.; Barbay, C.; Mer-Calfati, C.; Tranchant, N.; Arnault, J.C.; et al. Synchrotron Bragg diffraction imaging characterization of synthetic diamond crystals for optical and electronic power devices application. *J. Appl. Crystallogr.* **2017**, *50*, 561.

The XRT photographs by Shikata [42] produced much clearer images of the dislocations when he selected the (404) crystal plane in reflection mode for imaging. The XRT images generated across other crystallographic planes were less clear. Careful studies of the dislocations imaging in type Ib yellow-brown diamond crystals conducted by Shikata [42] showed that the dislocations are found to propagate in the <111> direction, with the major Burger vectors being in <110> and <1–10> directions. Many dislocations are also propagated in the <112> and <121> directions, although these are tilted with respect to <111> direction with a very slight angle (Figure 4). The dislocations are marked in Figure 4 and shown as dark spots in a line. If the dark spots are joined, they form a dark line. It can, therefore, be deduced that a dark line will indicate a higher density of dislocations in a sample. Based on this, we can conclude that the lower-right part of the sample plate (five o'clock position) in Figure 4 contains a higher density of dislocations. The dislocations with the same Burgers vector propagate in the same directions, but the dislocations are spread in a broad area. In the centre of many plates, a high density of dislocations is observed in an area of about 0.8 mm diameter, which may correspond to the initial seeds. The results

of Tran Thi [1] and Shikata [42] on the type Ib HPHT sample appear identical, with the difference that the image was much clearer in Shikata. The results in Figures 3 and 4 show point and line dislocations propagate along the <111> direction.

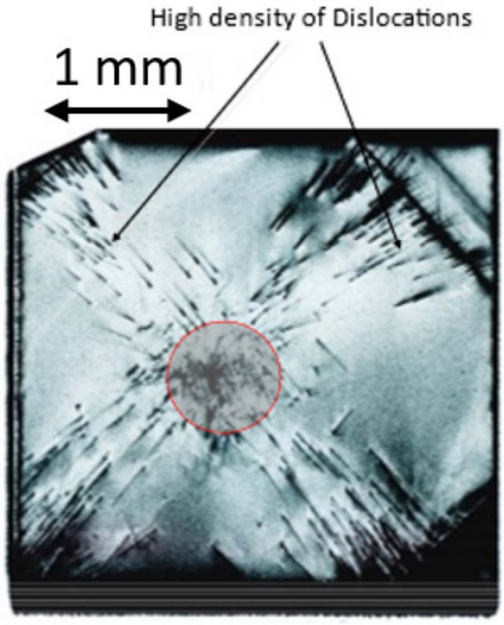


Figure 4. The X-ray topographic image of an HPHT type 1b single crystal diamond taken from the paper of Shikata [42]. The high density of dislocations is visible along the <111> and <112> directions. In the centre of the crystal, a circular region approximately 0.8 mm in diameter with a very high density of dislocations is visible. The size of the diamond plate is about 3 mm × 3 mm. The XRT image is taken in the (404) plane. Image is taken from ref. [42]: Shikata, S. Diamond dislocations analysis by X-ray topography. *Funct. Diam.* **2022**, *2*, 174. Reprinted by permission of Taylor & Francis Ltd, http://www.tandfonline.com (accessed on 1 February 2023) on behalf of Zhengzhou Research Institute for Abrasives & Grinding Co., Ltd.

In another study by Burns et al. [41], the white-beam XRT image of a yellow-brown crystal contains a large number of defects and lattice inhomogeneities. In particular, the boundaries between growth sectors exhibit substantial strain, and bundles of dislocations are typically found perpendicular to the (100) growth sectors lying in (110) or (111) crystallographic planes.

The rocking curve map of an HPHT type Ib crystal is shown in Figure 5. The image is produced in the (220) crystallographic plane. The high density of dislocations propagating along the <111> and <112> directions are visible as long, thick contrasts lines in the same manner as shown in Figures 3 and 4. While the XRT photograph directly shows the presence of dislocations and dislocation bundles as shown in Figures 3 and 4, the rocking curve map produces the variation in FWHM of the rocking curves at the locations where dislocations and dislocation bundles are present. A thick, long line here would imply a large density of dislocations represented by an increase in FWHM values of the rocking curve at the dislocation sites. The upper portion of Figure 5 shows a concentration of higher FWHM values, which implies a higher density of the dislocations in the sample in the upper-half portion. The FWHM values for the entire sample range from about 4 arc sec to 8 arc sec. There are a few advantages in conducting FWHM or rocking curve mapping of the samples. The FWHM is a more sensitive parameter than direct imaging, as imaging may not produce clear images all the time in all crystallographic planes. Rocking curve mapping can be measured for (111), (220) or (400) planes, and one can also learn about curvature or strain in the samples with rocking curve mapping [44].

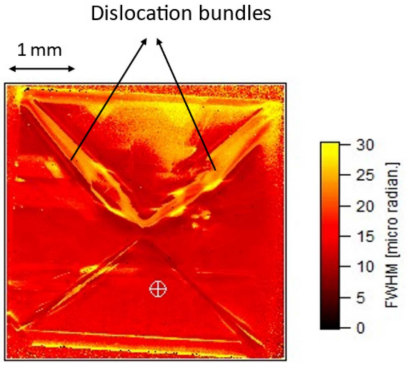


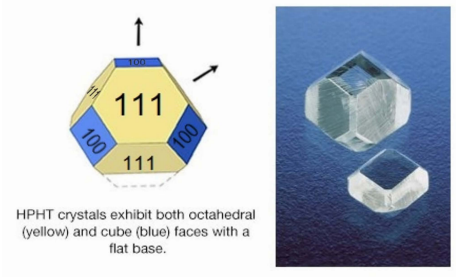
Figure 5. The FWHM map generated from the rocking curve map of a type 1b HPHT diamond plate of dimensions 5 mm × 5 mm in the (220) plane. The thick, long contrast lines support the results of Figure 3, implying a high density of dislocations propagating along the <111> direction. The centre of the crystal also has a high density of defects. The FWHM values for the entire sample range from about 4 arc sec to 8 arc sec (1 Micro radian = 0.206 arc sec). The scale bar is 1 mm.

3.2. HPHT SCDs (Type IIa)

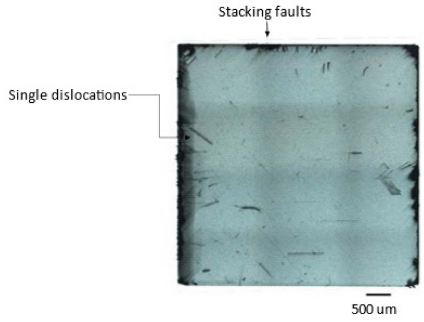
Type IIa SCDs produced by the HPHT method show the most perfect crystalline structure. The single crystal plates of type IIa SCDs show very few dislocations and minimum stacking faults. The concentration of nitrogen in type IIa diamond is very small (of the order of sub-parts per billion). This is achieved by using nitrogen getters and special techniques to reduce the uptake of nitrogen from the atmosphere and using catalysts and metals which are nitrogen-free. The seed which is used for the growth of type IIa HPHT SCDs is also selected very carefully with no defects and inhomogeneities. An image of a typical HPHT grown type IIa SCD is shown in Figure 6a, the crystal is white colour and would be of D colour on the GIA colour scale. The regular crystallographic planes visible on the crystal are (100), (110) and (111).

The first successful synthesis of high-quality type IIa HPHT SCDs was conducted by Sumiya et al. [26–28] using excellent quality, defect-free seeds. The SCDs showed a very high degree of crystalline perfection. The FWHM of the rocking curve, measured by a double crystal X-ray setup, was about 6 arc sec, and the cross-polarized images showed a complete absence of dislocations and dislocation bundles. In a later paper by Sumiya et al. [28], an XRT image of the crystal showed a perfect defect-free image of a type IIa HPHT diamond. The FWHM as measured by XRT was found close to the theoretical value of about 1 arc sec.

An XRT image of a type IIa plate taken from Shikata [42] is shown in Figure 6b. The topographic image of the type IIa plate is free of the defects and dislocations when compared with the topographic image of the type Ib crystal plates shown in Figures 3 and 4a, respectively. There are single dislocations and stacking faults at the edges; however, the high density of dislocations traversing along the <111> direction as observed in type Ib crystals (Figure 4) is absent. There are polishing lines, traversing along the diagonal direction, present on the surface of the plate as shown in Figure 6b. The image of an HPHT grown single crystal type IIa diamond (Figure 7) is taken from the paper of Burns et al. [41]. The white-beam XRT image in the (400) plane shows almost a perfect crystal with no dislocations in the centre portion of the crystal and only a few dislocations and stacking faults at the edge. The image of the dislocations on the edge on the right side of the crystal are not as high resolution because of low absorption of X-rays. Furthermore, this image is a white-beam XRT image. The stacking faults are clearly visible as a dark band in the upper portion of the image. The FWHM of the rocking curve map for this sample is about 1 arc sec, which is close to the theoretical value [41]. Shvydko et al. [43] showed an XRT image of 1 mm thick, almost flawless HPHT diamond plate for use in X-ray optics, which is a dominant application of type IIa HPHT diamond crystals.



(**a**)



(**b**)

Figure 6. The type IIa single crystal diamond produced by HPHT; the crystal is in cuboctahedral form and different crystal planes such as (100) and (111) are visible in (**a**). An X-ray topography image of a type IIa plate. Few line dislocations and stacking faults at the edge of the plate are seen (**b**). The size of the plate in (**b**) is about 3.5 mm × 3.5 mm. Image is taken from ref. [42]: Shikata, S. Diamond dislocations analysis by X-ray topography *Funct. Diam.* **2022**, *2*, 174. Reprinted by permission of Taylor & Francis Ltd, http://www.tandfonline.com (accessed on 1 February 2023) on behalf of Zhengzhou Research Institute for Abrasives & Grinding Co., Ltd.

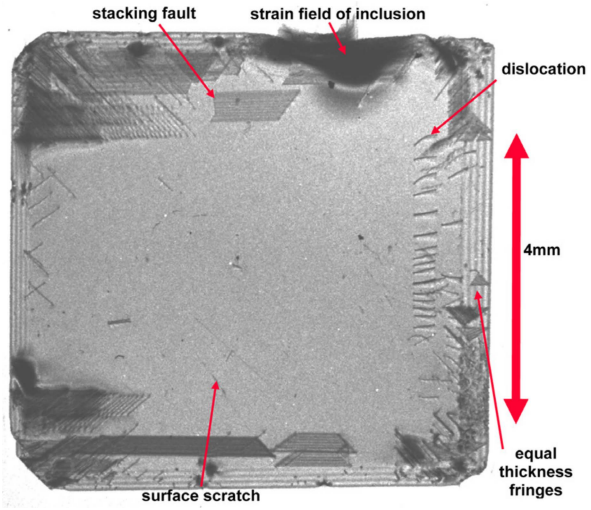
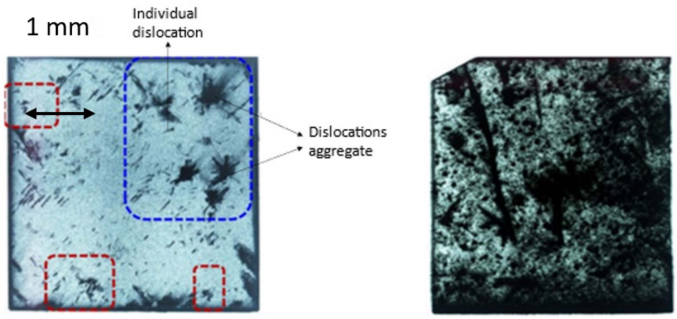


Figure 7. The white-beam topographic image of an HPHT grown type IIa single crystal (100) oriented plate from the paper of Burns et al. (ref. [41]). The centre portion of the crystal has almost no dislocations, and few dislocations are seen only on the side and stacking faults at the edges. The size of the plate is about 4 mm × 4 mm, and the FWHM of the rocking curve is approximately 1 arc sec. The image is taken from ref. [41]: Burns, R.C.; Chumakov, A.I.; Connel, S.H.; Dube, D.; Godfried, H.P.; Hansen, J.O.; Hartwig, J.; Hoszowska, J.; Massiello, F.; Mkhonza, L; et al. HPHT growth and X-ray characterization of high-quality type IIa diamond. *J. Phys. Condense. Matter* **2009**, *21*, 364224. Printed with permission from the publisher.

Recent images of a type IIa HPHT diamond crystal produced by Sumiya et al. [28] and New Diamond Technologies have shown perfect crystals which are free of dislocations and stacking faults in the centre portion. The process has been optimized to an extent where this is becoming a common feature. However, there are only a few groups that can produce such quality type IIa HPHT SCDs. In addition to the type IIa HPHT diamond crystals being dislocation-free, an additional significant characteristic is the lowest strain in the crystals. This makes them particularly suitable for X-ray optics and its applications.

3.3. CVD SCDs (Type IIa)

CVD SCDs have recently attracted a lot of attention due to their high application potential. Multiple groups [2,19,31–33,36–40,42,44,45] have studied the XRT images and rocking curve maps of CVD SCDs plates. XRT photographs as well as rocking curve maps of CVD plates show a much higher density of dislocation bundles. In addition, we commonly observe clusters of dislocation bundles forming dislocation aggregates. Shikata [42] has presented the results of XRT images of four commercially produced CVD single crystal diamond plates. One pair of CVD plates show fewer dislocation aggregates as compared to other pairs of plates, showing relatively large areas which are free of dislocation aggregates and defects. The other set, however, have a high density of dislocations aggregates and some dot-like bundles, which are of tens to hundreds of microns in size. The XRT photographs of the two representative plates are presented in Figure 8a,b. The dislocation aggregates are pointed to by black arrows within the blue and red areas. The aggregates have a range of dimensions from a few microns to hundreds of microns. In these aggregates, the analyses of dislocation propagation and the Burger vectors cannot be carried out, as the clusters of dislocations exist in the aggregates, and they appear randomly directed. The clusters form during growth and may be related to the quality of the substrates and their preparation. It is interesting that such aggregates are mostly absent in HPHT type Ib and type IIa diamond plates, as shown above. In type Ib and IIa HPHT crystals, only single dislocations and sometimes bundles of dislocations are observed. Some single dislocations also exist along with aggregates in Figure 8a. The presence of dislocation bundles and aggregates is much higher in the image of Figure 8b as compared to Figure 8a. The possible reason of the plate in Figure 8b having much higher aggregates and dislocation bundles may be the poor condition of the surface on which the growth occurred.



(**a**) (**b**)

Figure 8. The XRT photographs of the two CVD diamond plates taken from Shikata (ref. [42]). The plate in (**a**) shows aggregates of dislocations within the blue and red areas. Some single dislocations are also visible. In contrast, (**b**) has a much higher density of the dislocation aggregates and bundles. The image is taken in the (404) crystallographic plane and the dimensions of the plates are about 3.5 mm × 3.5 mm. The image is taken from ref. [42]: Shikata, S. Diamond dislocations analysis by X-ray topography. *Funct. Diam.* **2022**, *2*, 174. Reprinted by permission of Taylor & Francis Ltd, http://www.tandfonline.com (accessed on 1 February 2023) on behalf of Zhengzhou Research Institute for Abrasives & Grinding Co., Ltd.

The FWHM rocking curve images of two CVD plates for 220 crystallographic planes are shown in Figure 9a,b. These plates were used for the alpha particle detectors. The image shown in Figure 9a has an area which may be of good crystalline order. However, even in this region the presence of the dislocations is evident from the coloured bands. The lower-half portion of the sample plate in Figure 9a has a high density of dislocation bundles, evident from the thick lines. The rocking curve width scale for the sample (a) generates a value ranging from about 10 arc sec to 25 arc sec (1 Micro radian = 0.206 arc sec) for the entire sample. The average rocking curve width of the plate in Figure 9a is about 15 arc sec. In contrast, the CVD single crystal plate in Figure 9b shows a very high density of the dislocation aggregates.

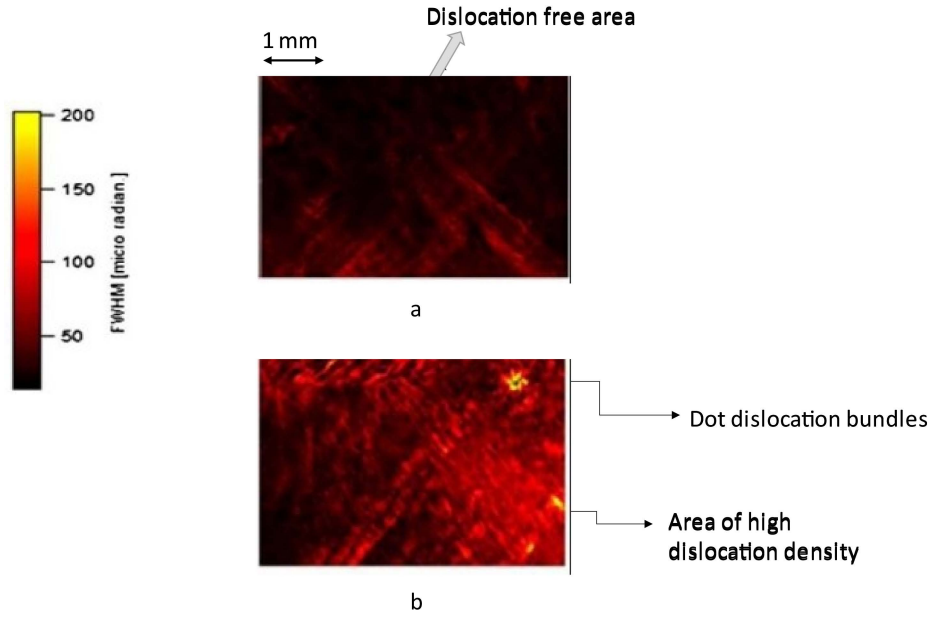


Figure 9. The rocking curve maps of two CVD single crystal diamond plates in (220) crystallographic planes; the part of the sample shown in (**a**) maybe of good crystallinity. However, even in this region the presence of dislocation bundles evident from coloured bands cannot be ruled out. The lower-half portion of the sample plate in (**a**) shows a high density of line dislocation evident from the thick lines. The sample in (**b**) shows a high density of dislocation aggregates. A dot-like structure full of dislocation bundles can also be seen in the upper-left corner of the image in (**b**). The size of the plates is approximately 5 mm × 4 mm. The image is taken from ref. [2]: Tarun, A.; Lee, S.J.; Yap, C.M.; Finkelstein, K.; Misra, D.S. Impact of impurities and crystal defects on the performance of CVD diamond detectors. *Diam. Rel. Mater.* **2016**, *63*, 169. Printed with permission from the publisher.

A dot-like structure full of dislocation bundles can also be seen in the upper-left corner of the image in Figure 9b. The size of this bundle is of the order of tens of microns, as also noted by Shikata [42]. The lower-right corner of the sample is full of the dislocation aggregates, and these have serious repercussions on the electronic properties of the CVD single crystal diamond plates, as discussed in later sections. The rocking curve width for the sample of the image in Figure 9b ranges from approximately 10 arc sec to 40 arc sec (1 Micro radian = 0.206 arc sec). It is interesting to note that the rocking curve map presented in Figure 9b conveys a similar structure as that presented in the XRT image in Figure 8b. The area of high dislocation density shown in Figure 9b contains a dislocation aggregates structure similar to those shown in Figure 8b as black clusters.

Yap et al. [19] found that the average rocking curve width of the ^{13}C doped samples increased nominally upon doping with a ^{13}C isotope of carbon. Further, the ^{13}C percentage was controlled by the feed gas composition of $^{13}CH_4$ and $^{12}CH_4$: $(^{13}CH_4)/(^{13}CH_4 + {}^{12}CH_4)$, and denoted by R. Samples were deposited with nominal R of 0.011 (natural abundance), 0.10, 0.21, 0.24 and 0.34. A rocking curve map of the sample grown with R = 0.24 is shown in

Figure 10. This should be compared with Figure 9a or b, which were grown with normal 6N purity CH_4 with natural presence of ^{13}C (R = 0.01). The rocking curve map was generated in the (220) crystallographic plane, and plate dimensions were 5 mm × 5 mm.

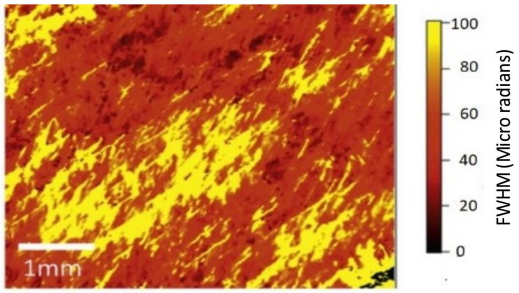


Figure 10. Rocking curve image of a ^{13}C doped single crystal diamond plate with R = 0.24. The image shows a general increase of dislocation bundles upon doping and an increase in average FWHM across the sample. The rocking curve map was generated along the (220) plane, and plate dimensions were approximately 5 mm × 5 mm. The image is from ref. [19]: Yap, C.M.; Tarun, A.; Xiao, S.; Misra, D S. MPCVD growth of ^{13}C-enriched diamond single crystals with nitrogen addition, *Diam. Rel. Mater*. **2016**, *63*, 2. Printed with permission from the Publisher.

It is evident from Figure 10 that there is a general increase of dislocation bundles, and the average rocking curve width has also increased across the entire sample when it is doped with ^{13}C. The FWHM values for this sample was found in the range of approximately 15 arc sec to approximately 45 arc sec (1 Micro radian = 0.206 arc sec). The rocking curve widths were found to increase by about 2.5% when R changed from 0.1 to 0.24.

A common difficulty associated with the CVD polycrystalline as well as single crystal diamond is the strain in the samples. When conducting rocking curve mapping, it is observed that the Bragg angle (θ) corresponding to a crystal plane shifts as one moves from one end of the sample plate to the other. Stoupin et al. [44] studied a set of 20 single crystal CVD diamond plates with rocking curve mapping using the CHESS synchrotron source (Figure 1). High dislocation density was present in all the samples. The average rocking curve widths were in the range of 30 arc sec–43 arc sec. The important result of the study was that they found distortions in the crystal lattice of all the plates. For 50% of the plates, the radius of the curvature was less than 10 m, which makes them unsuitable for application in X-ray monochromators. However, the remaining plates had a flat region in the centre of about few mm^2 area which had a radius of curvature greater than 30 m. These results suggested that the selected CVD diamond plates could be useful for X-ray monochromator applications. It is one advantage of rocking curve mapping that the shift in the theta (θ) value of the Bragg peak can be used to calculate the curvature and strain in the diamonds.

4. Discussion

Dislocations are present in large numbers in type Ib HPHT as well as CVD SCDs. In type Ib HPHT SCDs, the dislocations are mostly single dislocations and line dislocations. Occasionally, dislocation bundles can also be seen if the density of the dislocations is high. In contrast, the dislocations have a complex nature in CVD SCDs. The single dislocations and dislocation bundles are common occurrences in CVD SCDs. In many cases of CVD SCDs, however, the clusters of dislocations form dislocation aggregates, which are not seen in type Ib HPHT SCDs. These are illustrated in Figure 8a,b and Figure 9a,b. The difference could arise due to the different growth mechanism of the CVD and HPHT SCDs. In CVD growth, the diamond grows vertically on a substrate of the size, typically, of 5–6 mm, whereas in HPHT the diamond grows on a seed which is approximately 0.1 mm or 0.2 mm in size. In HPHT synthesis, the diamond grows with the help of a metal catalyst, while in CVD growth no catalyst is used. If we only compare the substrate size,

the equivalent of 30–50 seeds are used in CVD growth. This will obviously lead to the formation of lot more dislocations, dislocation bundles and clusters in CVD SCDs because most of these originate from the substrate [37,42,45]. Fujita et al. [48] showed that 45° dislocations are more energetically favourable to form in CVD SCDs. This is interesting because a superposition of several 45° dislocations can form clusters [49].

In contrast, the use of a metal catalyst in HPHT growth results in the regular cuboctahedron shape of type Ib HPHT crystals. CVD SCDs grow in cuboid shape. However, dislocations and dislocation bundles both are present in large numbers in HPHT type Ib SCDs as well. In type Ib HPHT SCDs, the dislocations originate from substrates as in CVD SCDs. However, one major difference between type Ib HPHT SCDs and CVD SCDs is the presence of substitutional nitrogen in the former. Substitutional nitrogen is a major impurity in type Ib HPHT SCDs, and its concentration may be as large as hundreds of ppm. The nitrogen impurities in HPHT SCDs lie mostly in (111) sectors [41], and it is no surprise that the large number of the dislocations in type Ib HPHT SCDs lie in the (111) planes. Obviously, the dislocations are tagged to the nitrogen impurity in type Ib HPHT SCDs. It is observed that the dislocation content of the CVD diamond layers grown on a type Ib HPHT substrate depends on the growth sector of HPHT seed crystals; (111) sectors of the CVD layer contain the highest concentration of both stacking faults and dislocations, but the (100) sectors are relatively free of both [42]. In type IIa HPHT SCDs, the seed is a perfect crystal and nitrogen impurity is not present; as a result, the dislocations and dislocation bundles are lowest in concentration.

The presence of dislocations and dislocation bundles plays a critical role in the application of the diamond layers. The charge collection efficiency (CCE) of the alpha particle detectors fabricated using single crystal CVD diamond deteriorates when there are large numbers of dislocation bundles present in the diamond layers [2–4,6]. The dislocation bundles generate internal strain in CVD SCDs, inhibiting its applications in high-pressure anvils. Low strain is an essential requirement of the SCDs which could be employed as anvils as demonstrated earlier by Ruaff and Vohra [50]. The presence of dislocation bundles in the epitaxial layers of the CVD SCDs layers is the main reason for the failure of vertical structure Schottky barrier diodes (SBDs) in high-power devices. SBDs fabricated on the diamond sample which had a large number of dislocation bundles exhibited inferior forward bias characteristics [42].

5. Conclusions and Future Work

In this paper the X-ray topography results of the various types of SCDs are reviewed. The dislocations and dislocation bundles are identified in rocking curve maps and XRT images. While in XRT images the dislocations and dislocation bundles can be easily observed as dark spots with a small tail, in rocking curve maps they are indirectly observed as an increase in the value of FWHM of the rocking curve. The conclusions of the study are as follows:

1. Dislocations and dislocation bundles are present in all types of SCDs, the only exception being the type IIa HPHT grown SCDs. The technology of growing HPHT type IIa SCDs has advanced to a level where the samples show almost no dislocations or dislocation bundles. However, it is important to understand that only very few groups have perfected that technology, and the dislocation-free type IIa HPHT samples are still scarcely available.
2. The line and point dislocations are present in type 1b HPHT SCDs, which have nitrogen impurities in the range of tens to hundreds ppm. If the dislocation density is high, the dislocations may fall in a line along the (111) or (112) directions. The dislocations may be related to the high concentration of nitrogen impurities in type 1b HPHT SCDs.
3. The centre of the type 1b HPHT plate appears to have dense dislocation bundles. Their origin may lie in the substrates used for the HPHT diamond growth.

4. While HPHT type Ib as well type IIa SCDs have mostly line dislocations, CVD SCDs appear to have point, line as well as aggregates of dislocations. The aggregate of dislocations is a big cluster of the dislocations. The dislocations as well as dislocation aggregates in CVD SCDs originate from the substrates.
5. In CVD SCDs, the dislocations originate from the substrates and travel within angular cones of 20–30 degrees. Therefore, one effective way of eliminating dislocations in CVD SCDs may be to use perfect substrates. Perfect substrates are difficult to define, but HPHT type IIa SCDs may be a good starting choice.
6. In CVD growth, the dislocations and aggregates also form during the growth and multiply. This results in a higher density of dislocations and dislocation bundles in CVD SCDs. A detailed optimization of the growth conditions is strongly needed to be performed in order to identify a parameter window in which dislocation-free growth may be possible on perfect substrates. This will be a direction for further work.
7. By using substrates which are free of dislocations and defects, it is possible to eliminate dislocations originating from substrates in CVD SCDs. Currently we do not know how to grow CVD SCDs free of all dislocations. There are a few important studies, however, of CVD diamond growth indicating control and elimination of the dislocations [38,45,51]. Elimination of all dislocations in CVD SCDs is a future research problem.

CVD single crystal diamond growth appears to be in the early stage in terms of dislocations and dislocation bundles, compared to other semiconductor wafers. The knowledge of dislocations is very critical for the applications of CVD single crystals, and urgent efforts must be made to grow dislocation- and defect-free CVD single crystals for the benefits of materials in various applications such as power electronics, MEMS, quantum electronics, anvils and other industrial applications.

The X-ray rocking curve measurements were conducted at the Cornell High Energy Synchrotron Source (CHESS) which is supported by the National Science Foundation and the National Institutes of Health/National Institute of General Medical Sciences under NSF award DMR-1332208. The assistance from CHESS Cornell and NSF (Alexandria, VA, USA), is gratefully acknowledged in this report.

Funding: We acknowledge support from IIa Technology for this work gratefully.

Data Availability Statement: The data is available within the manuscript.

Conflicts of Interest: Author declares no conflict of interest.

References

1. Tran Thi, T.N.; Morse, J.; Caliste, D.; Fernandez, B.; Eon, D.; Härtwig, J.; Barbay, C.; Mer-Calfati, C.; Tranchant, N.; Arnault, J.C.; et al. Synchrotron Bragg diffraction imaging characterization of synthetic diamond crystals for optical and electronic power devices application. *J. Appl. Crystallogr.* **2017**, *50*, 561–569. [CrossRef] [PubMed]
2. Tarun, A.; Lee, S.J.; Yap, C.M.; Finkelstein, K.; Misra, D.S. Impact of impurities and crystal defects on the performance of CVD diamond detectors. *Diam. Rel. Mater.* **2016**, *63*, 169–174. [CrossRef]
3. Berderman, E.; Pomorski, M.; De Boer, W.; Ciobanu, M.; Dunst, S.; Grah, C.; Kis, M.; Koenig, W.; Lange, W.; Lohmann, W. Diamond detectors for hadron physics research. *Diam. Rel. Mater.* **2010**, *19*, 358–367. [CrossRef]
4. Tallaire, A.; Mille, V.; Brinza, O.; Tran Thi, T.N.; Brom, J.M.; Loguinov, Y.; Achard, J. Thick CVD diamond films grown on high-quality type IIa HPHT diamond substrates from New Diamond Technology. *Diam. Rel. Mater.* **2017**, *77*, 146–152. [CrossRef]
5. Holly, C.; Traub, M.; Hoffmann, D.; Widmann, C.; Brink, D.; Nebel, C.; Gotthardt, G.; Sozbir, M.C.; Benzel, C. Monocrystalline CVD diamond optics for high power applications. In *High-Power Laser Materials Processing: Lasers, Beam Delivery, Diagnostics, and Applications V*; SPIE: Bellingham, WA, USA, 2016; Volume 9741, p. 974104.
6. Shimaoka, T.; Koizumi, S.; Kaneko, J. Recent progress in diamond radiation detectors. *Funct. Diam.* **2021**, *1*, 205–220. [CrossRef]
7. Shellaiah, M.; Sun, K.W. Diamond-Based Electrodes for Detection of Metal Ions and Anions. *Nanomaterials* **2022**, *12*, 64. [CrossRef]
8. Zhao, Y.; Li, C.; Liu, J.; An, K.; Yan, X.; Hei, L.; Chen, L.; Wei, J.; Lu, F. The Interface and Mechanical Properties of a CVD Single Crystal Diamond Produced by Multilayered Nitrogen Doping Epitaxial Growth. *Materials* **2019**, *12*, 2492. [CrossRef]
9. Wang, Y.; Zhang, W.; Lin, C.-N.; Ren, P.; Lu, Y.-J.; Shan, C.; Yu, S.F. Multiphoton Upconversion Emission from Diamond Single Crystal. *ACS Appl. Mater. Interfaces* **2018**, *10*, 18935–18941. [CrossRef]

10. Shellaiah, M.; Chen, T.H.; Simon, T.; Li, L.-C.; Sun, K.W.; Ko, F.-H. An Affordable Wet Chemical Route to Grow Conducting Hybrid Graphite-Diamond Nanowires: Demonstration by A Single nanowire Device. *Sci. Rep.* **2017**, *7*, 11243. [CrossRef] [PubMed]
11. Shellaiah, M.; Chen, T.H.; Simon, T.; Li, L.-C.; Sun, K.W.; Ko, F.-H. Effect of Metal Ions on Hybrid Graphite-Diamond Nanowire Growth: Conductivity Measurements From a Single Nanowire Device. *Nanomaterials* **2019**, *9*, 415. [CrossRef] [PubMed]
12. Chrenko, R. ^{13}C-doped diamond: Raman spectra. *J. Appl. Phys.* **1988**, *63*, 5873. [CrossRef]
13. Banholzer, W.F.; Anthony, T.R. Isotope Enrichment During Diamond Growth. *Diam. Rel. Mater.* **1992**, *1*, 1157–1160. [CrossRef]
14. Laraoui, A.; Dolde, F.; Burk, C.; Reinhard, F.; Wrachtrup, J.; Meriles, C. High-resolution correlation spectroscopy of ^{13}C spins near a nitrogen-vacancy centre in diamond. *Nat. Commun.* **2013**, *4*, 1651. [CrossRef]
15. Scharfenberger, B.; Munro, W.J.; Kae, N. Coherent control of a NV^{-} centre near one adjacent 13C. *New J. Phys.* **2014**, *16*, 093043. [CrossRef]
16. Dréau, A.; Maze, J.-R.; Lesik, M.; Roch, J.-F.; Jacques, V. High-resolution spectroscopy of single NV defects coupled with nearby ^{13}C nuclear spins in diamond. *Phys. Rev. B* **2012**, *85*, 134107–134114. [CrossRef]
17. Qiu, W.; Velisavljevic, N.; Baker, P.; Vohra, Y.; Weir, S. Calibration of an isotopically enriched C-13 layer pressure sensor to 156 GPa in a diamond anvil cell. *Appl. Phys. Lett.* **2004**, *84*, 5308–5310. [CrossRef]
18. Novikov, N.; Podoba, A.; Shmegera, S.; Witek, A.; Zaitsev, A.; Denisenko, A.; Fahrner, W.; Werner, M. Influence of Isotopic Content On Diamond Thermal Conductivity. *Diam. Rel. Mater.* **1999**, *8*, 1602–1606. [CrossRef]
19. Yap, C.M.; Tarun, A.; Xiao, S.; Misra, D.S. MPCVD growth of ^{13}C-enriched diamond single crystals with nitrogen addition. *Diam. Rel. Mater.* **2016**, *63*, 2–11. [CrossRef]
20. Lang, A.R. Dislocations in diamond and the origin of trigons. *Proc. Roy. Soc. A* **1964**, *278*, 234.
21. Lang, A.R. Causes of Birefringence in Diamond. *Nature* **1967**, *213*, 248. [CrossRef]
22. Lang, A.R.; Moore, M.; Makepeace, A.P.W. On the dilation of synthetic type Ib diamond by substitutional nitrogen impurity. *Philos. Trans. Roy. Soc. A* **1991**, *337*, 497.
23. Lang, A.R. Topographic methods for studying defects in diamonds. *Diam. Rel. Mater.* **1993**, *2*, 106–114. [CrossRef]
24. Lang, A.R. X-ray topographic and optical imaging studies of synthetic diamond. *J. Appl. Crystallogr.* **1994**, *27*, 988–1001. [CrossRef]
25. Wierzchowsky, W.; Moore, M. Bragg-case images of stacking faults. *Acta Cryst. A* **1995**, *51*, 831–840. [CrossRef]
26. Sumiya, H.; Toda, N.; Nishibayashi, Y.; Satoh, S. Crystalline perfection of high purity synthetic diamond crystal. *J. Cryst. Growth* **1997**, *178*, 485–494. [CrossRef]
27. Sumiya, H.; Tamasaku, K. Large defect-free synthetic type IIa diamond crystals synthesized via high pressure and high temperature. *Jpn. J. Appl. Phys.* **2012**, *51*, 090102–090105. [CrossRef]
28. Sumiya, H.; Harano, K.; Tamasaku, K. HPHT synthesis and crystalline quality of large high-quality (001) and (111) diamond crystals. *Diam. Rel. Mater.* **2015**, *58*, 221. [CrossRef]
29. Macrander, A.T.; Krasnicki, S.; Zhong, Y.; Maj, J.; Chu, Y.S. Strain mapping with parts-per-million resolution in synthetic type Ib diamond plates. *Appl. Phys. Lett.* **2005**, *87*, 194113. [CrossRef]
30. Moore, M.; Nailer, S.G.; Wierzchowski, W. Optical and X-ray Topographic Studies of Dislocations, Growth-Sector Boundaries and Stacking Faults in Synthetic Diamonds. *Crystal* **2016**, *6*, 71. [CrossRef]
31. Gaukroger, M.; Martineau, P.; Crowder, M.; Friel, I.; Williams, S.; Twitchen, D.J. X-ray topography studies of dislocations in single crystal CVD diamond. *Diam. Rel. Mater.* **2008**, *17*, 262–269. [CrossRef]
32. Martineau, P.; Gaukroger, M.P.; Guy, K.B.; Lawson, S.C.; Twitchen, D.J.; Friel, I.; Hansen, J.O.; Summerton, G.C.; Addison, T.P.G.; Burns, R. High crystalline quality single crystal chemical vapour deposition diamond. *J. Phys. Condens. Matter* **2009**, *21*, 362417. [CrossRef]
33. Finkelstein, K.; Jones, R.; Pauling, A.; Brown, Z.; Tarun, A.; Jupitz, S.; Sagan, D.; Misra, D.S. Monochromatic X-ray Topographic Capability at CHESS. 2016. Available online: http://news.chess.cornell.edu/articles/2015/Finkelstein151123.html (accessed on 7 April 2023).
34. Tamasaku, K.; Ueda, T.; Miwa, D.; Ishikawa, T. Goniometric and topographic characterization of synthetic type IIa diamonds. *J. Phys. D Appl. Phys.* **2005**, *38*, A61. [CrossRef]
35. Tsoutsouva, M.; Oliveira, V.; Baruchel, J.; Camel, D.; Marie, B.; Lafford, T. Characterization of defects in mono-like silicon for photovoltaic applications by Bragg diffraction imaging. *J. Appl. Crystallogr.* **2015**, *48*, 645–654. [CrossRef]
36. Yang, G.L.; Jones, R.; Klein, F.; Finkelstein, K.; Livingston, K. Rocking Curve Imaging For Diamond Radiator Crystal Selection. *Diam. Rel. Mater.* **2010**, *19*, 719–722. [CrossRef]
37. Prokhorov, I.; Ralchenko, V.; Bolshakov, A.; Polskiy, A.; Vlasov, A.; Subbotin, I.; Podurets, K.; Pashaev, E.; Sozontov, E. Analysis of synthetic diamond single crystals by X-ray topography and double crystal diffractometry. *Crystallogr. Rep.* **2013**, *58*, 1010–1016. [CrossRef]
38. Boussadi, A.; Tallaire, A.; Kasu, M. Reduction of dislocation densities in single crystal CVD diamond by confinement in the lateral sector. *Diam. Rel. Mater.* **2018**, *83*, 162–169. [CrossRef]
39. Masuya, S.; Kasu, M. Dislocations in chemical vapor deposition (111) single crystal diamond observed by synchrotron X-ray topography and their relation with etch pits. *Diam. Rel. Mater.* **2018**, *90*, 40–46. [CrossRef]

40. Umezawa, H.; Kato, Y.; Watanabe, H.; Omer, A.; Yamaguchi, H.; Shikata, S. Characterization of crystallographic defects in homoepitaxial diamond films by synchrotron X-ray topography and cathodoluminescence. *Diam. Rel. Mater.* **2011**, *20*, 523–526. [CrossRef]
41. Burns, R.C.; Chumakov, A.I.; Connel, S.H.; Dube, D.; Godfried, H.P.; Hansen, J.O.; Hartwig, J.; Hoszowska, J.; Massiello, F.; Mkhonza, L.; et al. HPHT growth and x-ray characterization of high-quality type IIa diamond. *J. Phys. Condense. Matter* **2009**, *21*, 364224–364237. [CrossRef] [PubMed]
42. Shikata, S. Diamond dislocations analysis by X-ray topography. *Funct. Diam.* **2022**, *2*, 174. [CrossRef]
43. Shvydko, Y.; Blank, V.; Terentyev, S. Diamond X-ray optics: Transparent, resilient, high-resolution and waveform preserving. *MRS Bull.* **2017**, *42*, 437–444. [CrossRef]
44. Stoupin, S.; Krawczyk, T.; Liu, Z.; Franck, C. Selection of CVD Diamond Crystals for X-ray Monochromator Applications Using X-ray Diffraction Imaging. *Crystals* **2019**, *9*, 396–406. [CrossRef]
45. Wang, R.; Lin, F.; Niu, G.; Su, J.; Yan, X.; Wei, Q.; Wang, W.; Wang, K.; Yu, C.; Wang, H.-X. Reducing Threading Dislocations of CVD Single Crystal Diamond via In Situ Tungsten Incorporation. *Materials* **2022**, *15*, 444. [CrossRef] [PubMed]
46. Luo, T.; Lindner, L.; Blinder, R.; Capelli, M.; Langer, J. Rapid determination of single substitutional nitrogen N^0_s concentration in diamond from UV-Vis spectroscopy. *Appl. Phys. Lett.* **2022**, *121*, 064002. [CrossRef]
47. Kazuchits, V.N.; Kazuchits, N.M.; Rusetskiy, M.S.; Korolik, O.V.; Konovalova, A.V.; Ignatenko, O.V. Rapid HPHT annealing of Synthetic Ib-type Diamond. *Carbon* **2021**, *174*, 180. [CrossRef]
48. Fujita, N.; Blumenau, A.T.; Jones, R.; Oberg, S.; Briddon, P.R. Theoretical studies on <100> dislocations in single crystal CVD diamond. *Phys. Status Solidi* **2006**, *203*, 3070–3075.
49. Pinto, H.; Jones, R. Theory of the birefringence due to dislocations in single crystal CVD diamond. *J. Phys. Condense. Matter* **2009**, *21*, 364220–364227. [CrossRef]
50. Ruaff, A.L.; Vohra, Y.K. Multimegabar Pressure Using Synthetic Diamond Anvils. *Appl. Phys. Lett.* **1989**, *55*, 232. [CrossRef]
51. Li, F.; Zhang, J.; Wang, X.; Zhang, M.; Wang, H. Fabrication of Low Dislocation Density, Single-Crystalline Diamond via Two-Step Epitaxial Lateral Overgrowth. *Crystals* **2017**, *7*, 114. [CrossRef]

Disclaimer/Publisher's Note: The statements, opinions and data contained in all publications are solely those of the individual author(s) and contributor(s) and not of MDPI and/or the editor(s). MDPI and/or the editor(s) disclaim responsibility for any injury to people or property resulting from any ideas, methods, instructions or products referred to in the content.